Surface Science Spectra

RESEARCH ARTICLE | MARCH 06 2026

Manganese ferrite films by chemical vapor deposition, analyzed by x-ray photoelectron spectroscopy

Alessandro Bigiani ; Chiara Maccato ; Gian Andrea Rizzi ; Davide Barreca

Surf. Sci. Spectra 33, 014006 (2026)
https://doi.org/10.1116/6.0005242

SSS SURFACE SCIENCE SPECTRA ARTICLE pubs.aip.org/avs/sss

Manganese ferrite films by chemical vapor deposition, analyzed by x-ray photoelectron spectroscopy

Cite as: Surf. Sci. Spectra 33, 014006 (2026); doi: 10.1116/6.0005242
Submitted: 17 December 2025 · Accepted: 20 February 2026 ·
Published Online: 6 March 2026

Alessandro Bigiani,[1] Chiara Maccato,[1] Gian Andrea Rizzi,[1] and Davide Barreca[2,a)]

AFFILIATIONS

[1]Department of Chemical Sciences, Padova University and INSTM, 35131 Padova, Italy
[2]CNR-ICMATE and INSTM, Department of Chemical Sciences, Padova University, 35131 Padova, Italy

[a)]**Electronic mail:** davide.barreca@unipd.it.

ABSTRACT

Manganese iron oxide ($MnFe_2O_4$), an environmentally friendly material, has been the subject of numerous studies for a broad range of technological end-uses. In the present work, we focus on an x-ray photoelectron spectroscopy investigation of a representative $MnFe_2O_4$ specimen grown by chemical vapor deposition on fluorine-doped tin oxide. The material was fabricated starting from homologous β-diketonate diamine Mn(II) and Fe(II) molecular precursors in an $O_2 + H_2O$ atmosphere, followed by *ex situ* annealing in an inert atmosphere. Beside the survey scan, we present and discuss high-resolution C 1*s*, O 1*s*, Mn 2*p*, Mn 3*s*, and Fe 2*p* spectra, recorded using a monochromated Al K_α x-ray source. Our findings provide valuable comparative data for researchers working on the preparation and characterization of manganese ferrite-containing systems for a wide range of applications.

Accession#: 02072
Technique: XPS
Specimen: $MnFe_2O_4$ fabricated by CVD
Instrument: ThermoFisher Scientific EscalabTM QXi
Major Elements in Spectra: C, O, Mn, and Fe
Minor Elements in Spectra: None
Published Spectra: 7
Spectral Category: Comparison

INTRODUCTION

Ternary spinel ferrites, an important class of multimetal oxides of general formula MFe_2O_4, have attracted a considerable attention worldwide thanks to their amenable catalytic, electrical, optical, and magnetic properties, which pave the way to numerous technological end-uses (Refs. 1–3). In fact, such systems feature multifaceted applications thanks to the broad variety of compositions and morphologies, whose control provides a powerful tool to engineer material characteristics and behavior (Ref. 1). In this context, manganese ferrite ($MnFe_2O_4$)-based systems have drawn a remarkable interest for several end-uses, among which the most recently targeted include catalysts for gaseous/aqueous pollutant degradation (Refs. 4–8), electrochemical capacitors (Refs. 9 and 10), and electrocatalysts for the oxygen evolution reaction (OER) and the oxygen reduction reaction (Refs. 11–19).

Since the physicochemical and functional properties of manganese ferrite materials are directly dependent on the adopted fabrication route and processing conditions (Refs. 19 and 20), many works have been addressed at the preparation of $MnFe_2O_4$ systems by means of different techniques (Refs. 16 and 21). Despite significant progresses have been achieved in this regard, further investigation focused on $MnFe_2O_4$ design, preparation, and thorough characterization is still needed in order to fully exploit the potential of this important material class (Ref. 17).

In the framework of our ongoing research activities, we report herein on the synthesis of $MnFe_2O_4$ systems by chemical vapor deposition (CVD) on fluorine-doped tin oxide (FTO) substrates, in view of their possible use as electrodes for the OER process in water splitting to yield green hydrogen. The target systems were obtained starting from $M(hfa)_2TMEDA$ complexes (with M = Mn,

Fe; Hhfa = 1,1,1,5,5,5-hexafluoro-2,4-pentanedione; TMEDA = *N*,*N*,*N*′,*N*′-tetramethylethylenediamine), previously used as precursors for the preparation of single-metal iron and manganese oxides (Refs. 22–24). Prior to the deposition process, thermal analyses were performed on the single $M(hfa)_2TMEDA$ compounds and their mixtures to ascertain the consistency of their vaporization rates for their use as "single-source" precursor of manganese ferrite. The data indicated a unique vaporization step for the two adducts, which were then used in a stoichiometric Mn:Fe = 1:2 molar ratio for the CVD of $MnFe_2O_4$. In particular, the present study is focused on a detailed x-ray photoelectron spectroscopy (XPS) characterization of a representative sample, yielding important information on the chemical states of the different elements. The analyses revealed a predominance of Mn^{2+} and Fe^{3+}, along with an appreciable content of oxygen vacancies, potentially beneficial for (electro)catalytic applications. These findings may pave the way to further research, expanding the applicative potential of these materials across various fields.

SPECIMEN DESCRIPTION [ACCESSION # 02072]

Specimen: $MnFe_2O_4$ grown by CVD at 400 °C
CAS Registry #: 12063-10-4
Specimen Characteristics: Homogeneous; solid; polycrystalline; semiconductor; inorganic compound; film
Chemical Name: Manganese iron oxide (spinel ferrite)
Source: Specimen prepared by CVD on FTO at 400 °C for 120 min, followed by thermal treatment under flowing nitrogen at 500 °C for 1 h.
Composition: Mn, Fe, and O
Form: Supported film
Structure: X-ray diffraction analyses revealed, beside peaks pertaining to the FTO substrate, the occurrence of signals located at $2\theta \approx 30°$ and ≈35°, corresponding to the (220) and (311) reflections typical of the *jacobsite* cubic spinel structure (Ref. 25). Transmission electron microscopy and related analyses confirmed $MnFe_2O_4$ presence. Field emission-scanning electron microscopy evidenced a uniform deposit morphology, characterized by globular nanoparticles (mean size ≈ 20 nm) assembled into bigger agglomerates (average dimensions ≈ 230 nm).
History and Significance: FTO substrates (Aldrich®; ≈7 Ω/sq; FTO thickness ≈ 600 nm) were precleaned according to a previously reported procedure (Ref. 24). $Mn(hfa)_2TMEDA$ and $Fe(hfa)_2TMEDA$ precursors were prepared as described in earlier publications (Refs. 26–28). Depositions were performed in a custom-made horizontal, hot-wall reactor (Ref. 29) under reduced pressure. The preground precursor mixture [total weight = 0.30 g (0.10 g $Mn(hfa)_2TMEDA$; 0.20 g $Fe(hfa)_2$-TMEDA)] was vaporized at 70 °C in an external glass reservoir and transported into the reaction chamber by an electronic-grade N_2 flow [rate = 100 standard cubic centimeters per minute (SCCM)], through gas lines heated at 120 °C by means of external tapes. A water-vapor-saturated oxygen flow (rate = 30 SCCM), used as reacting gas, was introduced through an independent inlet. The following deposition settings were used: reactor temperature = 400 °C; overall pressure = 3 mbar; process duration = 120 min. Before characterization, the sample was subjected to annealing under nitrogen at 500 °C for 1 h (heating rate = 20 °C/min) and slowly cooled down to room temperature.
As Received Condition: As grown
Analyzed Region: Same as the host material
***Ex Situ* Preparation/Mounting:** The specimen was fixed on a grounded sample holder by metallic clips and introduced into the analysis chamber through a fast entry system.
***In Situ* Preparation:** The sample was analyzed as-received.
Charge Control: None
Temp. During Analysis: 298 K
Pressure During Analysis: $<10^{-7}$ Pa
Pre-analysis Beam Exposure: 150 s

INSTRUMENT DESCRIPTION

Manufacturer and Model: ThermoFisher Scientific EscalabTM QXi
Analyzer Type: Spherical sector
Detector: Channeltron
Number of Detector Elements: 6

INSTRUMENT PARAMETERS COMMON TO ALL SPECTRA

Spectrometer

Analyzer Mode: Constant pass energy
Throughput ($T = E^N$): The transmission function is calculated from a cubic polynomial fit to a plot of log[peak area/(PE × XSF)] vs log(KE/PE), where PE, KE, and XSF indicate the pass energy, the kinetic energy, and the relative sensitivity factor (Refs. 30 and 31).
Excitation Source Window: None
Excitation Source: Al K_α monochromatic
Source Energy: 1486.6 eV
Source Strength: 200 W
Source Beam Size: $400 \times 200\ \mu m^2$
Signal Mode: Single channel direct

Geometry

Incident Angle: 58°
Source-to-Analyzer Angle: 58°
Emission Angle: 0°
Specimen Azimuthal Angle: 90°
Acceptance Angle from Analyzer Axis: ±45°
Analyzer Angular Acceptance Width: 60° × 10°

Ion Gun

Manufacturer and Model: ThermoFisher Scientific MAGCIS Dual Beam Ion Source
Energy: 4000 eV
Current: 7 mA
Current Measurement Method: Biased stage
Sputtering Species and Charge: Ar^+
Spot Size (unrastered): 500 μm
Raster Size: $4500 \times 4500\ \mu m^2$

Incident Angle: 45°
Polar Angle: 45°
Azimuthal Angle: 90°
Comment: Differentially pumped ion gun

DATA ANALYSIS METHOD

Energy Scale Correction: No binding energy (BE) scale correction was necessary.
Recommended Energy Scale Shift: 0 eV
Peak Shape and Background Method: Peak positions and widths were determined by fitting the spectra using mixed Gaussian/Lorentzian functions, after a Shirley-type background subtraction (Ref. 32).
Quantitation Method: Atomic concentrations were calculated by peak area integration, using sensitivity factors from the ALTHERMO1 library as provided in the ThermoScientific Avantage software (version 6.9.1, Build 00004).

ACKNOWLEDGMENTS

Padova University (P-DiSC#02BIRD2023-UNIPD RIGENERA, DOR 2023–2025), INSTM Consortium (TRI.25/013—CIMENTO), and PRIN 2022474YE8 (SCI-TROPHY project; Next Generation EU—Bando PRIN 2022—M4.C2.1.1) are gratefully acknowledged for financial support. Thanks are also due to Alberto Gasparotto (Department of Chemical Sciences, Padova University, Italy) and to Marzio Rancan (CNR-ICMATE, Padova, Italy) for valuable discussions and technical support.

AUTHOR DECLARATIONS

Conflict of Interest

The authors have no conflict to disclose.

Author Contributions

Alessandro Bigiani: Investigation (equal); Methodology (equal); Visualization (equal); Writing – original draft (equal); Writing – review & editing (equal). **Chiara Maccato:** Formal analysis (equal); Methodology (equal); Supervision (lead); Visualization (equal); Writing – review & editing (lead). **Gian Andrea Rizzi:** Conceptualization (equal); Data curation (equal); Formal analysis (equal); Funding acquisition (equal); Investigation (equal); Methodology (equal); Supervision (lead); Visualization (equal); Writing – review & editing (equal). **Davide Barreca:** Conceptualization (equal); Data curation (equal); Formal analysis (equal); Funding acquisition (equal); Investigation (equal); Visualization (equal); Writing – original draft (equal); Writing – review & editing (equal).

DATA AVAILABILITY

The data that support the findings of this study are available within the article and its supplementary material.

REFERENCES

[1]P. K. Baruah, N. Mukherjee, B. Bhagat, and K. Mukherjee, Cryst. Growth Des. **24**, 1504 (2024).
[2]R. Nepal, M. Saghayezhian, J. Zhang, and R. Jin, J. Magn. Magn. Mater. **497**, 165955 (2020).
[3]D. Peeters *et al.*, ACS Sustain. Chem. Eng. **5**, 2917 (2017).
[4]Z. Cheng, S. Luo, X. Li, S. Zhang, T. Thang Nguyen, M. Guo, and X. Gao, Appl. Surf. Sci. **566**, 150654 (2021).
[5]A. Kumar, M. K. Gora, G. Lal, B. L. Choudhary, P. L. Meena, R. S. Dhaka, R. K. Singhal, S. Kumar, and S. N. Dolia, Environ. Sci. Pollut. Res. **30**, 18820 (2023).
[6]L. Liu, J. Sun, J. Ding, Y. Zhang, T. Sun, and J. Jia, Inorg. Chem. **58**, 13241 (2019).
[7]Y. Fu, P. Xiong, H. Chen, X. Sun, and X. Wang, Ind. Eng. Chem. Res. **51**, 725 (2012).
[8]M. R. Rajani, R. Ravishankar, K. Maya Naik, M. Srinidhi Raghavan, C. Vidya, S. Girish Kumar, and C. Manjunatha, Appl. Surf. Sci. Adv. **16**, 100434 (2023).
[9]G. Singh and S. Chandra, Int. J. Hydrogen Energy **43**, 4058 (2018).
[10]A. Sivakumar, S. Sahaya Jude Dhas, P. Sivaprakash, A. I. Almansour, R. Suresh Kumar, N. Arumugam, K. Perumal, S. Arumugam, and S. A. Martin Britto Dhas, J. Inorg. Organomet. Polym. Mater. **32**, 344 (2022).
[11]M. Chen, N. Kitiphatpiboon, C. Feng, Q. Zhao, A. Abudula, Y. Ma, K. Yan, and G. Guan, Appl. Catal., B: Environ. **330**, 122577 (2023).
[12]A. R. C. Bredar, M. D. Blanchet, A. R. Burton, B. E. Matthews, S. R. Spurgeon, R. B. Comes, and B. H. Farnum, ACS Catal. **12**, 3577 (2022).
[13]J. X. Flores-Lasluisa, D. Salinas-Torres, M. V. López-Ramón, C. Moreno-Castilla, M. A. Álvarez, E. Morallón, and D. Cazorla-Amorós, Environ. Res. **204**, 112126 (2022).
[14]J. Kim, J. Lee, C. Liu, S. Pandey, S. Woo Joo, N. Son, and M. Kang, Appl. Surf. Sci. **546**, 149124 (2021).
[15]A. Kumar, B. N. Mahanty, A. Rawat, R. Muhammad, R. K. Panigrahi, D. Pradhan, and P. Mohanty, Energy Fuels **37**, 6810 (2023).
[16]T. Pandiarajan, S. Ravichandran, and L. J. Berchmans, RSC Adv. **4**, 64364 (2014).
[17]M. Tang, Y. Zou, Z. Jiang, P. Ma, Z. Zhou, X. Zhu, J. Bao, and S.-G. Sun, J. Energy Chem. **97**, 12 (2024).
[18]Y. Zhou, Y. Du, S. Xi, and Z. J. Xu, Electrocatalysis **9**, 287 (2018).
[19]H. Guermazi, M. Smari, A. Tahir, M. Y. Haik, T. Mnasri, T. Haq, and Y. Haik, Int. J. Hydrogen Energy **157**, 150468 (2025).
[20]C. Murugesan, K. Ugendar, L. Okrasa, J. Shen, and G. Chandrasekaran, Ceram. Int. **47**, 1672 (2021).
[21]L. Gao, Z. Liu, Z. Yang, L. Cao, C. Feng, M. Chu, and J. Tang, Appl. Surf. Sci. **508**, 145292 (2020).
[22]T. Wagner, D. Valbusa, L. Bigiani, D. Barreca, A. Gasparotto, and C. Maccato, Surf. Sci. Spectra **27**, 024004 (2020).
[23]G. Carraro, A. Gasparotto, C. Maccato, and D. Barreca, Surf. Sci. Spectra **20**, 9 (2013).
[24]D. Barreca *et al.*, Int. J. Hydrogen Energy **38**, 14189 (2013).
[25]PDF card n° 73-1964 (2002).
[26]D. Barreca *et al.*, Dalton Trans. **41**, 149 (2012).
[27]D. Barreca, G. Carraro, A. Gasparotto, C. Maccato, R. Seraglia, and G. Tabacchi, Inorg. Chim. Acta **380**, 161 (2012).
[28]C. Maccato *et al.*, Chem. - A Eur. J. **23**, 17954 (2017).
[29]D. Barreca, G. Carraro, A. Gasparotto, C. Maccato, C. Sada, E. Bontempi, M. Brisotto, O. Pliekhova, and U. L. Štangar, Environ. Sci. Pollut. Res. **23**, 20350 (2016).
[30]M. Benedet, A. Gasparotto, G. A. Rizzi, C. Maccato, D. Mariotti, R. McGlynn, and D. Barreca, Surf. Sci. Spectra **30**, 024018 (2023).
[31]K. M. Cole, D. W. Kirk, and S. J. Thorpe, Surf. Sci. Spectra **28**, 014001 (2021).
[32]D. A. Shirley, Phys. Rev. B **5**, 4709 (1972).
[33]See http://srdata.nist.gov/xps for BE reference values; accessed November 2025.
[34]J. F. Moulder, W. F. Stickle, P. E. Sobol, and K. D. Bomben, *Handbook of X-Ray Photoelectron Spectroscopy* (Perkin Elmer Corporation, Eden Prairie, MN, 1992).

[35]F. Mattelaer, T. Bosserez, J. Rongé, J. A. Martens, J. Dendooven, and C. Detavernier, RSC Adv. **6**, 98337 (2016).
[36]L. Bigiani, C. Maccato, D. Barreca, and A. Gasparotto, Surf. Sci. Spectra **27**, 024005 (2020).
[37]E. Beyreuther, S. Grafström, L. M. Eng, C. Thiele, and K. Dörr, Phys. Rev. B **73**, 155425 (2006).
[38]Y. Konno, T. Yamamoto, and T. Nagayama, Nanoscale **13**, 12738 (2021).

SPECTRAL FEATURES TABLE

Spectrum ID #	Element/ Transition	Peak Energy (eV)	Peak Width FWHM (eV)	Peak Area (eV × cts/s)	Sensitivity Factor	Concentration (at. %)	Peak Assignment
02072-02[a]	C 1*s*	284.8	1.5	72 727.8	1.000	15.7	Adventitious contamination
02072-02[a]	C 1*s*	286.3	1.6	11 947.5	1.000	2.6	C–O species from precursor residuals
02072-02[a]	C 1*s*	288.4	1.8	8446.1	1.000	1.8	Oxidized C-containing species from adventitious contamination
02072-03[b]	O 1*s*	530.1	1.4	4 41 241.4	2.881	36.8	Lattice oxygen in $MnFe_2O_4$
02072-03[b]	O 1*s*	531.8	1.9	1 54 950.2	2.881	12.9	Chemisorbed –OH and oxidized C-containing species
02072-04[c]	Mn 2*p*	…	…	4 86 352.6	12.353	10.0	Mn in $MnFe_2O_4$
02072-04	Mn $2p_{3/2}$	641.4	2.9	…	…	…	Mn in $MnFe_2O_4$
02072-04	Mn $2p_{1/2}$	653.1	3.0	…	…	…	Mn in $MnFe_2O_4$
02072-05	Mn 3*s*	…	…	20 404.3	…	…	Mn in $MnFe_2O_4$
02072-05	Mn $3s_1$	83.0	2.7	…	…	…	Mn in $MnFe_2O_4$
02072-05	Mn $3s_2$	89.1	2.3	…	…	…	Mn in $MnFe_2O_4$
02072-06[d]	Fe 2*p*	…	…	10 90 142.7	14.353	20.2	Fe in $MnFe_2O_4$
02072-06	Fe $2p_{3/2}$	711.2	3.5	…	…	…	Fe in $MnFe_2O_4$
02072-06	Fe $2p_{1/2}$	724.9	4.0	…	…	…	Fe in $MnFe_2O_4$

[a]The sensitivity factor is referred to the whole C 1*s* signal.
[b]The sensitivity factor is referred to the whole O 1*s* signal.
[c]The peak area, sensitivity factor, and concentration are referred to the whole Mn 2*p* signal.
[d]The peak area, sensitivity factor, and concentration are referred to the whole Fe 2*p* signal.

Footnote to Spectrum 02072-01: The wide-scan spectrum revealed the presence of Mn, Fe, and O photoelectron and Auger signals, as expected, as well as of carbon peaks. No fluorine contamination arising from the used metal precursors was ever observed.

Footnote to Spectrum 02072-02: The C 1*s* signal was composed of three distinct bands. The main one at the lowest energy value (284.8 eV) was related to adventitious carbon due to environmental exposure. The lower intensity components located at 286.3 and 288.4 eV were ascribed to C–O species from precursor residuals and oxidized C-containing species from adventitious contamination, respectively (Refs. 3, 4, 22, 33, and 34).

Footnote to Spectrum 02072-03: The O 1*s* peak showed the presence of two components. The most intense one, centered at 530.1 eV, was assigned to lattice oxygen in $MnFe_2O_4$ (Refs. 6, 11, and 14), whereas the second one at 531.8 eV was attributed to –OH groups chemisorbed on oxygen vacancies (Refs. 3, 17, and 34). Nevertheless, the second component also resulted from oxidized C-containing species from adventitious contamination (Refs. 33 and 34). Excluding the latter contribution, a stoichiometry close to $MnFe_2O_{3.7}$ is obtained. As a matter of fact, the occurrence of oxygen vacancies may be beneficial in view of eventual catalytic end-uses of the target materials (Refs. 6, 11, and 13). No molecularly adsorbed water was detected.

Footnote to Spectrum 02072-04: The Mn 2*p* signal shape and position [BE(Mn $2p_{3/2}$) = 641.4 eV; spin–orbit splitting (SOS) = 11.7 eV] were in agreement with previously reported literature data for $MnFe_2O_4$ (Refs. 7, 15, and 20). In particular, the *shake-up* satellites located at ≈645 and ≈659 eV indicate the predominance of Mn(II) (Refs. 2, 12, 13, and 21). This conclusion was in line with the energy difference (Δ) between the Mn $2p_{3/2}$ component and the lower BE O 1*s* band (Δ = 111.3 eV), which pointed out to a formal Mn oxidation state very close to +2 (Ref. 35). Yet, the occurrence of Mn(III) in low amounts could not be unambiguously ruled out, whereas the occurrence of Mn (IV) could be excluded based on a comparison with previous literature data (Refs. 5 and 36).

Footnote to Spectrum 02072-05: The Mn 3*s* signal was split into two components due to multiplet splitting, arising from the presence of unpaired electrons in the manganese valence level (Ref. 22). In this case, the component separation was estimated to be 6.1 eV, a value which, in tune with the above findings, indicated an average manganese valence state very close to +2 (Refs. 11 and 37).

Footnote to Spectrum 02072-06: The Fe 2*p* photopeak features [BE (Fe $2p_{3/2}$) = 711.2 eV; SOS = 13.7 eV], indicating that the majority of iron in the target sample possesses the +3 valence state, as also confirmed by the satellites at ≈719.3 and ≈733.1 eV (Refs. 5, 11, 13, 17, 21, 33, and 38), are consistent with previous literature reports on $MnFe_2O_4$ (Refs. 4, 12, 15, and 20).

ANALYZER CALIBRATION TABLE

Spectrum ID #	Element/ Transition	Peak Energy (eV)	Peak Width FWHM (eV)	Peak Area (eV × cts/s)	Sensitivity Factor	Concentration (at. %)	Peak Assignment
…	Au $4f_{7/2}$	84.0	1.1	28 41 305.7	11.593	…	Au(0)
…	Ag $3d_{5/2}$	368.3	0.9	13 16 206.9	13.068	…	Ag(0)
…	Cu $2p_{3/2}$	932.7	1.3	53 50 621.8	18.147	…	Cu(0)

Comment to Analyzer Calibration Table: The peaks were acquired after Ar^+ erosion.

GUIDE TO FIGURES

Spectrum (Accession) #	Element/Transition	Voltage Shift	Multiplier	Baseline	Comment #
02072-01	Survey	0	1	0	…
02072-02	C 1*s*	0	1	0	…
02072-03	O 1*s*	0	1	0	…
02072-04	Mn 2*p*	0	1	0	…
02072-05	Mn 3*s* + Fe 3*s*	0	1	0	…
02072-06	Fe 2*p*	0	1	0	…
02072-07	Valence	0	1	0	…

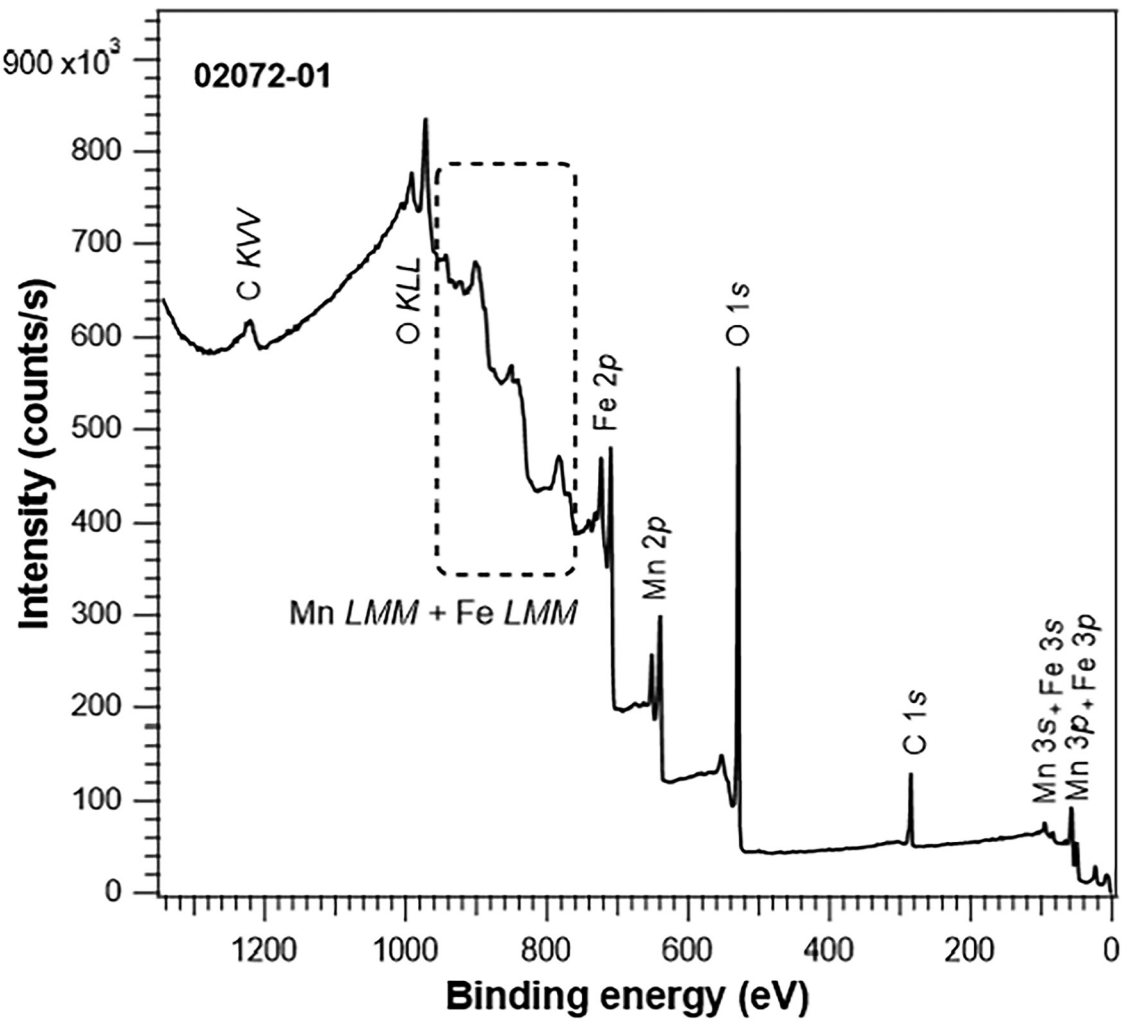

Accession #:	02072-01
■ Specimen:	$MnFe_2O_4$
■ Technique:	XPS
■ Spectral Region:	Survey
Instrument:	ThermoFisher Scientific Escalab Xi
Excitation Source:	Al K_α monochromatic
Source Energy:	1486.6 eV
Source Strength:	200 W
Source Size:	$400 \times 200\ \mu m^2$
Analyzer Type:	Spherical sector analyzer
Incident Angle:	58°
Emission Angle:	0°
Analyzer Pass Energy:	100 eV
Instrument Resolution:	1.0 eV
Total Signal Accumulation Time:	204.2 s
Total Elapsed Time:	224.6 s
Number of Scans:	3

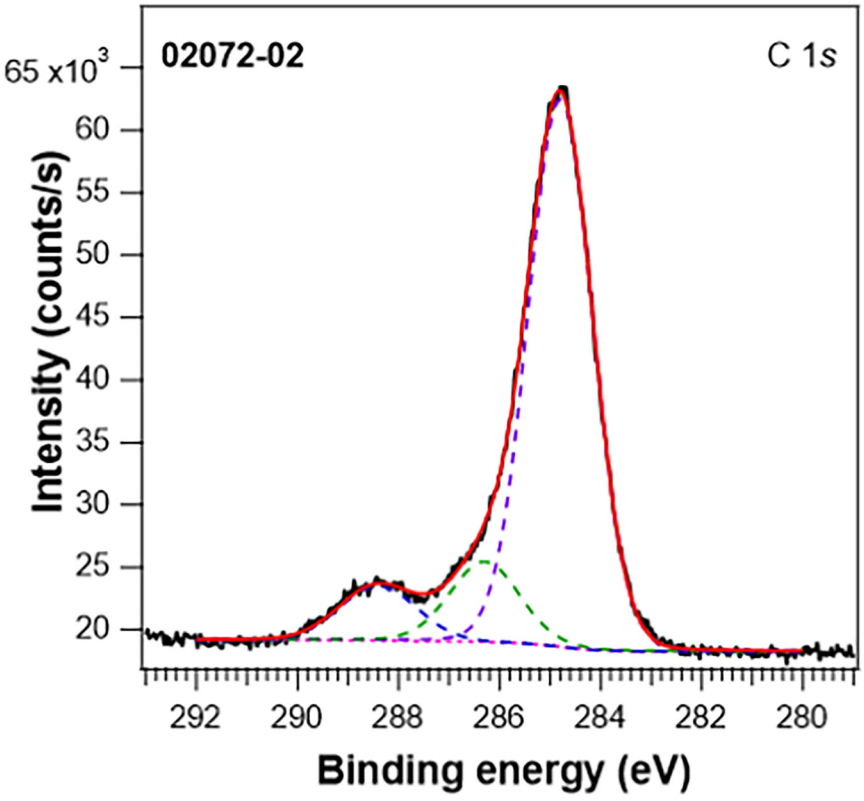

- **Accession #:** 02072-02
- **Specimen:** $MnFe_2O_4$
- **Technique:** XPS
- **Spectral Region:** C 1*s*

Instrument: ThermoFisher Scientific Escalab Xi
Excitation Source: Al K_α monochromatic
Source Energy: 1486.6 eV
Source Strength: 200 W
Source Size: 400 × 200 μm^2
Analyzer Type: Spherical sector
Incident Angle: 58°
Emission Angle: 0°
Analyzer Pass Energy: 50 eV
Instrument Resolution: 0.5 eV
Total Signal Accumulation Time: 100.1 s
Total Elapsed Time: 110.1 s
Number of Scans: 2

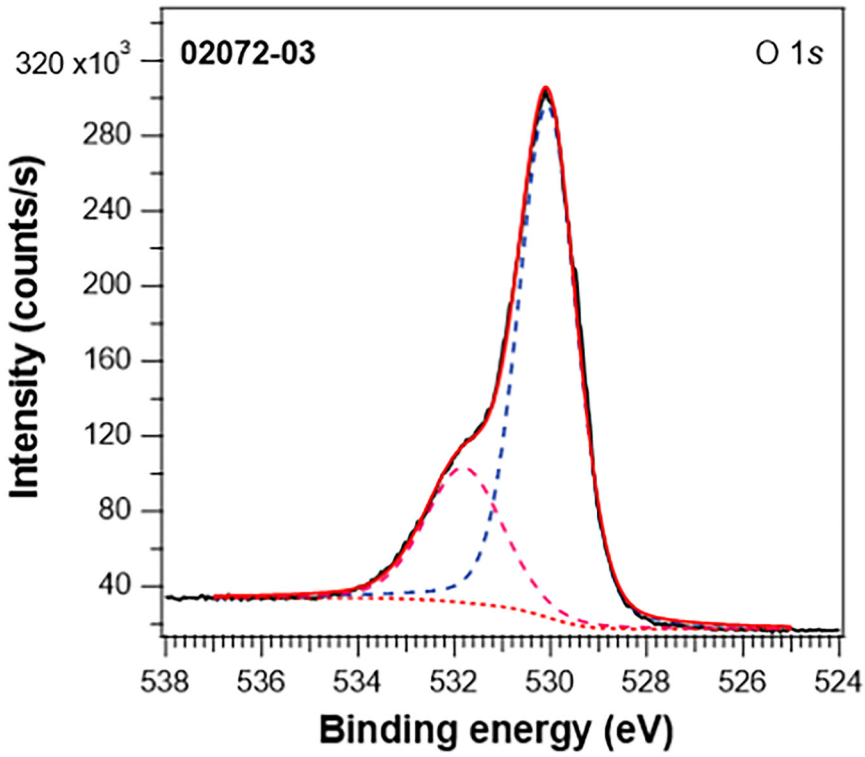

- **Accession #:** 02072-03
- **Specimen:** $MnFe_2O_4$
- **Technique:** XPS
- **Spectral Region:** O 1*s*

Instrument: ThermoFisher Scientific Escalab Xi
Excitation Source: Al K_α monochromatic
Source Energy: 1486.6 eV
Source Strength: 200 W
Source Size: 400 × 200 μm^2
Analyzer Type: Spherical sector
Incident Angle: 58°
Emission Angle: 0°
Analyzer Pass Energy: 50 eV
Instrument Resolution: 0.5 eV
Total Signal Accumulation Time: 50.1 s
Total Elapsed Time: 55.1 s
Number of Scans: 1

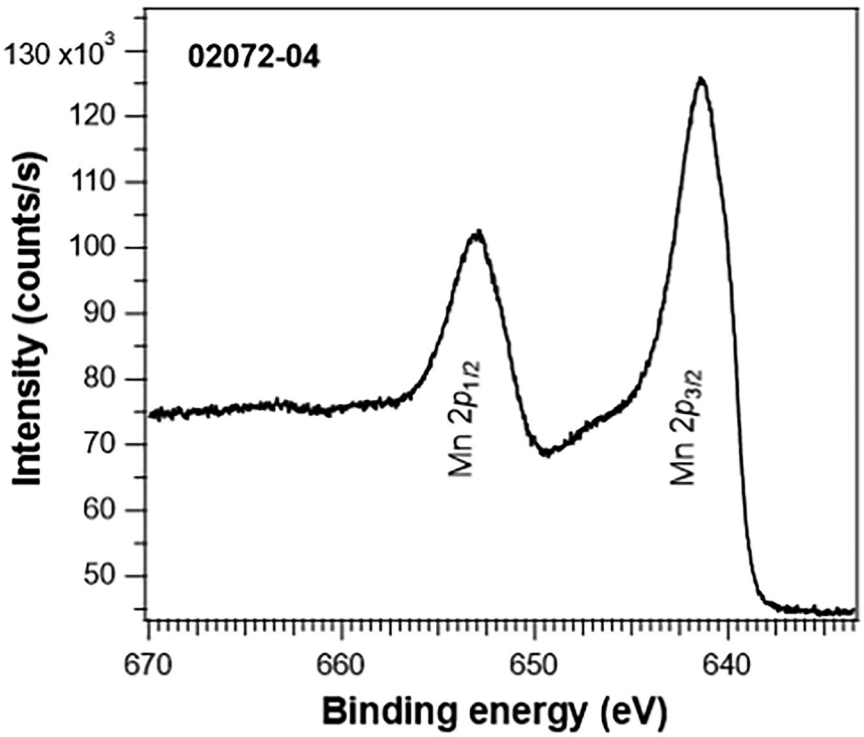

- **Accession #:** 02072-04
- **Specimen:** $MnFe_2O_4$
- **Technique:** XPS
- **Spectral Region:** Mn 2*p*

Instrument: ThermoFisher Scientific Escalab Xi
Excitation Source: Al K_α monochromatic
Source Energy: 1486.6 eV
Source Strength: 200 W
Source Size: 400 × 200 μm^2
Analyzer Type: Spherical sector
Incident Angle: 58°
Emission Angle: 0°
Analyzer Pass Energy: 50 eV
Instrument Resolution: 0.5 eV
Total Signal Accumulation Time: 380.2 s
Total Elapsed Time: 418.2 s
Number of Scans: 4

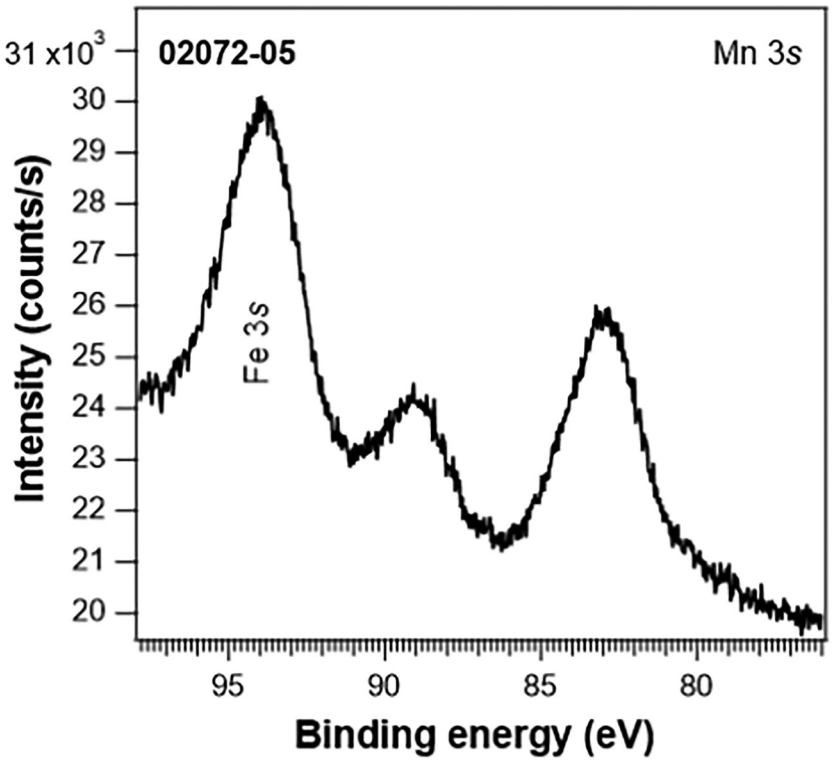

- **Accession #:** 02072-05
- **Specimen:** $MnFe_2O_4$
- **Technique:** XPS
- **Spectral Region:** Mn 3*s* + Fe 3*s*

Instrument: ThermoFisher Scientific Escalab Xi
Excitation Source: Al K_α monochromatic
Source Energy: 1486.6 eV
Source Strength: 200 W
Source Size: 400 × 200 μm^2
Analyzer Type: Spherical sector
Incident Angle: 58°
Emission Angle: 0°
Analyzer Pass Energy: 50 eV
Instrument Resolution: 0.5 eV
Total Signal Accumulation Time: 825.5 s
Total Elapsed Time: 908.1 s
Number of Scans: 10

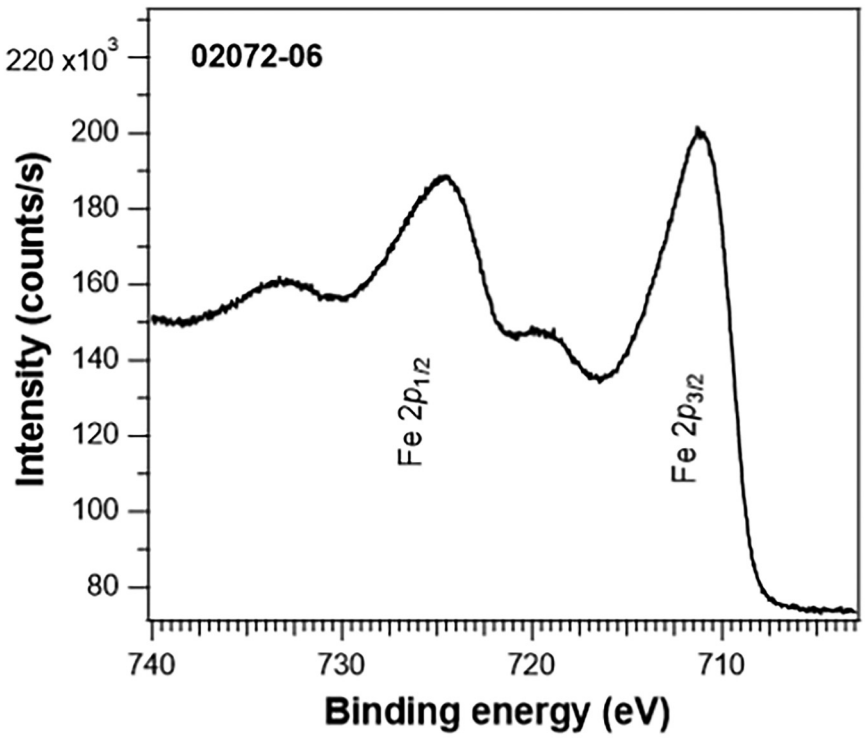

- **Accession #:** 02072-06
- **Specimen:** $MnFe_2O_4$
- **Technique:** XPS
- **Spectral Region:** Fe 2*p*

Instrument: ThermoFisher Scientific Escalab Xi
Excitation Source: Al K_α monochromatic
Source Energy: 1486.6 eV
Source Strength: 200 W
Source Size: 400 × 200 μm^2
Analyzer Type: Spherical sector
Incident Angle: 58°
Emission Angle: 0°
Analyzer Pass Energy: 50 eV
Instrument Resolution: 0.5 eV
Total Signal Accumulation Time: 400.2 s
Total Elapsed Time: 440.2 s
Number of Scans: 4

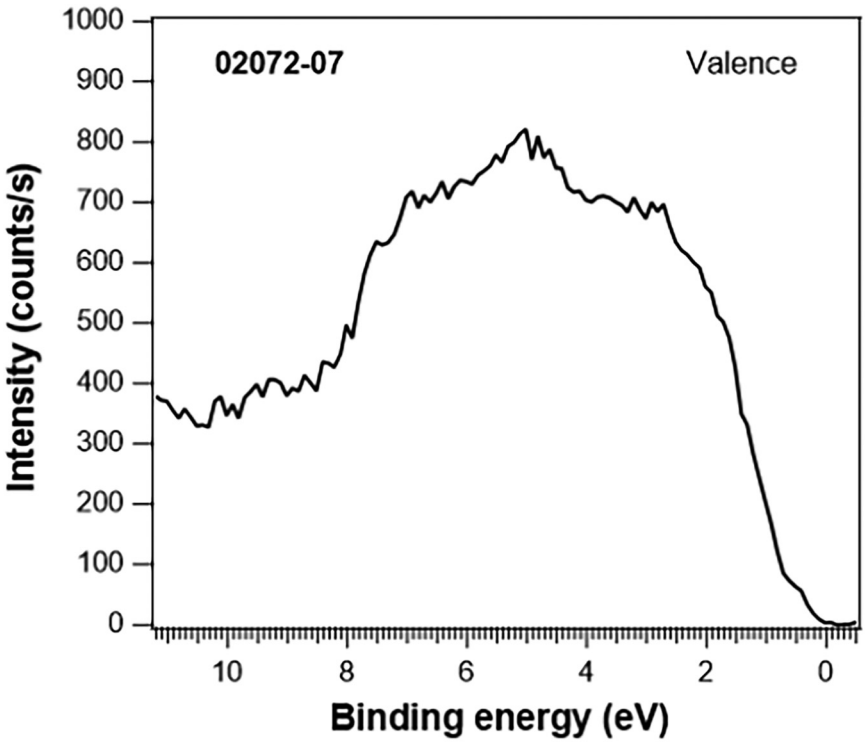

- **Accession #:** 02072-07
- **Specimen:** $MnFe_2O_4$
- **Technique:** XPS
- **Spectral Region:** Valence

Instrument: ThermoFisher Scientific Escalab Xi
Excitation Source: Al K_α monochromatic
Source Energy: 1486.6 eV
Source Strength: 200 W
Source Size: 400 × 200 μm^2
Analyzer Type: Spherical sector
Incident Angle: 58°
Emission Angle: 0°
Analyzer Pass Energy: 10 eV
Instrument Resolution: 0.1 eV
Total Signal Accumulation Time: 392.0 s
Total Elapsed Time: 431.2 s
Number of Scans: 20